Measuring the thermal resistance of vertical interfaces separating two different media using lock-in infrared thermography with laser spot heating

J. González[1,2], A. Bedoya[1,3], A. Mendioroz[1] and A. Salazar[1]

[1]Departamento de Física Aplicada I, Escuela de Ingeniería de Bilbao, Universidad del País Vasco UPV/EHU, Plaza Ingeniero Torres Quevedo 1, 48013 Bilbao, Spain.

[2]Department of Applied Physics, CINVESTAV Unidad Mérida, carretera Antigua a Progreso km 6, A.P. 73 Cordemex, Mérida Yucatán 97310, Mexico.

[3]Instituto Politécnico Nacional (IPN), Centro de Investigación en Ciencia Aplicada y Tecnología Avanzada (CICATA), Unidad Legaria, Legaria 694, Col. Irrigación, C.P. 11500, Ciudad de México, Mexico.

E-mail: agustin.salazar@ehu.es

Abstract

We propose a method to measure the thermal contact resistance at the vertical interface between two materials using lock-in infrared thermography with laser spot heating. We found an analytical expression for the surface temperature of the two media when one of them is illuminated by a modulated and focused laser spot. We analyzed how the thermal conductivities of the two-media affect the sensitivity to the interface thermal resistance. We concluded that the key factor is the product of both thermal conductivities: the higher this product, the lower the thermal resistance that can be detected. The surface temperature of two media with calibrated interface thickness is measured using an infrared camera. The thermal resistance of the interface is obtained by fitting the surface temperature to the analytical model. The good agreement between the nominal and retrieved width of the interface confirmed the validity of the model.

Keywords: infrared thermography, lock-in infrared thermography, crack detection, thermal waves, analytical solution, nondestructive evaluation.

1. Introduction

Detecting and characterizing narrow vertical cracks is a challenge for conventional nondestructive testing methods like dye penetrant, magnetic particles, eddy currents, ultrasonics and x-ray. Since the pioneering work by Kubiak [1] infrared (IR) thermography has been applied as a noncontact, nonintrusive and health safe method to detect near-surface defects. Ultrasound excited thermography (vibrothermography), has been used to detect closed fissures, which absorb the acoustic energy conveyed by the ultrasound waves and convert it into heat. This heat propagates toward the surface, indicating the presence of the defect on a cold background (for a recent comprehensive review see Ref. 2 and references therein). However, the main drawback of this technique is that the ultrasonic transducer must be in contact with the sample, which reduces its versatility. In a similar way, induction thermography uses electromagnetic pulses to launch eddy currents in electrical conductors. The eddy currents generate heat by resistive losses in the material. Subsurface flaws produce local changes of the electrical current densities, which become visible in the thermographic images [3,4]. Although it is noncontact, it is restricted to electrical conducting samples.

Optically stimulated thermography is noncontact and applies to any kind of material, but the presence of the defect produces just a perturbation of the existing surface temperature field generated by the optical excitation. Moreover, the spatial shape of the illumination strongly affects the detectability of defects. In the case of vertical cracks, if the sample is excited by a homogeneous illumination producing a heat flux perpendicular to the sample surface, the crack will barely disperse the heat flux thus producing a negligible signature on the surface temperature distribution. Accordingly, to detect vertical cracks an asymmetry in the heat flux must be produced: A laser spot is focused close to the crack, whose thermal resistance partially blocks the heat flux, thus inducing an asymmetry in the temperature field at both sides of the fissure. This method was first used for imaging the presence of cracks [5-7]. In the last years, several approaches to characterize the crack (depth, length and width) have been developed. For instance, by solving numerically the heat diffusion equation in a homogeneous sample containing a vertical crack, the depth of the crack is retrieved [8-10]. On the other hand, analytical solutions of the surface temperature can be obtained for infinite cracks. By fitting the surface temperature measured by an infrared camera to the model, the thermal resistance of the crack is obtained [11-15].

In this work, we deal with the characterization of the thermal contact resistance at the vertical interface between two different media. We propose a method based on laser spot excitation close to the interface and using lock-in infrared thermography, which provides amplitude and phase thermograms with a very low noise level. As we consider infinite interfaces, we have found an analytical expression for the surface temperature. In previous works dealing with the interface between two materials, the surface temperature was calculated using Green functions [11,16]. In this work, we take advantage of the Hankel transform [17] to obtain simple analytical solutions. Due to the different thermal properties of the two materials, a singularity in the amplitude and phase of the temperature appears at the interface, even if the thermal contact is perfect. The lack of thermal contact at the interface adds a discontinuity (a jump) in both amplitude and phase of the temperature. The goal is to measure the thermal contact resistance R_{th} at the interface, which quantifies its width. To do this, we fit a temperature profile across the interface to the analytical model. We have found that the key factor for detecting narrow interfaces is the product of the thermal conductivities of both materials: the higher this product, the lower the thermal resistance that can be detected. To verify the method, we have prepared calibrated infinite vertical interfaces by inserting thin metallic tapes (down to 1 μm thick) between two blocks of different materials. A modulated cw-laser beam is focused close to the crack. An IR video camera, equipped with a lock-in module, provides the amplitude

and phase of the surface temperature around the crack. We fit the temperature profile crossing the center of the laser spot and perpendicular to the interface to obtain R_{th}. The agreement between the thickness of the metallic tapes and the retrieved R_{th} confirms the validity of the method, which could be useful to characterize the junction between two solids (e.g. welding) or in the quality control of contacts between different parts of composite materials.

It is worth mentioning that this method can be used with other photothermal techniques sensing a quantity proportional to the surface temperature like photothermal reflectance [18]. This technique allows using high modulation frequencies (MHz) together with tightly focused laser beams (spot diameter ≈ 1 μm), thus sensing the temperature field at micrometer scale. Accordingly, the method proposed in this manuscript opens the way to size the thermal resistance at grain boundaries in composite materials (in the range of $R_{th} = 10^{-9}$-10^{-8} m^2K/W), which are responsible for reducing the thermal conductivity due to the scattering of heat carriers at the interfaces [15,19].

2. Theory

Let us consider two semi-infinite and opaque materials placed in contact through an infinite vertical interface placed at plane $y = 0$. Medium 1 is at $y < 0$ and medium 2 is at $y > 0$. The surface of medium 2 is illuminated by a laser beam of power P_o, modulated at a frequency f ($\omega = 2\pi f$). The center of the Gaussian laser spot is located at a distance d from the interface and its radius is a (at $1/e^2$ of the maximum intensity). The geometry of the problem is shown in Fig. 1. We assume adiabatic boundary conditions at the sample surfaces, i.e. heat losses by convection and radiation to the surroundings are neglected. The aim is to calculate the surface temperature (amplitude and phase) distribution. To do this, we proceed in three steps: (a) First, we calculate the temperature due to a point-like heat source and infinite media, (b) then, we include the effect of the free surface at $z = 0$ and (c) finally, we take into account the effect of the Gaussian profile of the heat source.

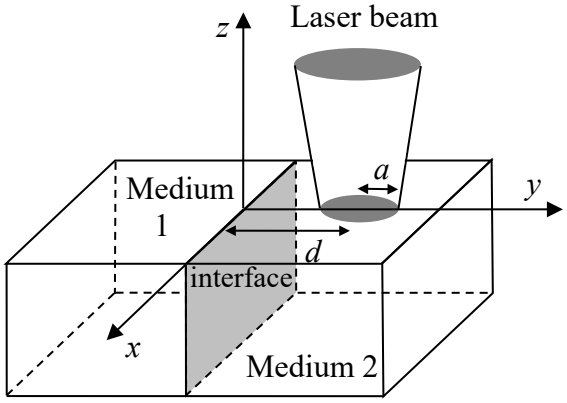

Figure 1. Geometry of the problem showing the vertical interface (in grey) between medium 1 and 2 and illuminated by a Gaussian laser beam.

We start considering a point-like heat source of modulated power $P(t) = \frac{P_o}{2}\left[1 + \cos(\omega t)\right]$ located at (0,d,0) and infinite media 1 and 2, i.e. without free surface at $z = 0$. The expressions for the spherical thermal wave T generated at the heat source, and the thermal waves scattered at the interface travelling through medium 2 and through medium 1, τ_2 and τ_1 respectively, are given by [13,20]

$$T(x,y,z)=\frac{P_o}{4\pi K_2}\frac{e^{-q_2R}}{R}=\frac{P_o}{4\pi K_2}\int_0^\infty \delta J_o(\delta r)\frac{e^{-\beta_2|y-d|}}{\beta_2}d\delta\,, \tag{1}$$

$$\tau_1(x,y,z)=P_o\int_0^\infty \delta J_o(\delta r)Ae^{\beta_1 y}d\delta\,, \tag{2}$$

$$\tau_2(x,y,z)=P_o\int_0^\infty \delta J_o(\delta r)Be^{-\beta_2 y}d\delta\,, \tag{3}$$

where $q_j=\sqrt{i\omega/D_j}$ is the thermal wave vector, $\beta_j=\sqrt{\delta^2+q_j^2}$, with subscript j = 1,2. K and D the thermal conductivity and diffusivity of the material respectively, J_o is the Bessel function of order zero, $R=\sqrt{x^2+(y-d)^2+z^2}$ and $r=\sqrt{x^2+z^2}$. Note that the last expression in Eq. (1) represents a spherical thermal wave in the Hankel space.

The temperature of material 1 and 2 is given by $T_1=\tau_1$ and $T_2=T+\tau_2$ respectively. Moreover, the values of A and B are determined from the boundary conditions at the interface: heat flux continuity and temperature discontinuity due to the lack of thermal contact:

$$-K_1\left.\frac{dT_1}{dy}\right|_{y=0}=-K_2\left.\frac{dT_2}{dy}\right|_{y=0} \tag{4}$$

$$(T_2-T_1)_{y=0}=R_{th}K_2\left.\frac{dT_2}{dy}\right|_{y=0}\,, \tag{5}$$

where R_{th} is the thermal contact resistance at the interface, which is related to the air gap width L through the equation $R_{th}=L/K_{air}$ [21]. By solving Eqs. (4) and (5) we obtain

$$A=\frac{e^{-\beta_2 d}}{2\pi}\times\frac{1}{K_1\beta_1+K_2\beta_2+R_{th}K_1\beta_1K_2\beta_2}. \tag{6b}$$

$$B=\frac{e^{-\beta_2 d}}{4\pi K_2\beta_2}\times\frac{-K_1\beta_1+K_2\beta_2+R_{th}K_1\beta_1K_2\beta_2}{K_1\beta_1+K_2\beta_2+R_{th}K_1\beta_1K_2\beta_2}, \tag{6a}$$

Accordingly, the temperature inside each material is given by

$$T_1(x,y,z)=\frac{P_o}{2\pi}\int_0^\infty \delta J_o(\delta r)e^{\beta_1 y}e^{-\beta_2 d}f_1(\delta)d\delta\,, \tag{7a}$$

$$T_2(x,y,z)=\frac{P_o}{4\pi K_2}\int_0^\infty \delta J_o(\delta r)\frac{e^{-\beta_2|y-d|}}{\beta_2}d\delta+\frac{P_o}{4\pi}\int_0^\infty \delta J_o(\delta r)e^{-\beta_2 y}e^{-\beta_2 d}f_2(\delta)d\delta\,, \tag{7b}$$

where

$$f_1(\delta)=\frac{1}{K_1\beta_1+K_2\beta_2+R_{th}K_1\beta_1K_2\beta_2}, \tag{8a}$$

$$f_2(\delta)=\frac{1}{K_2\beta_2}\times\frac{-K_1\beta_1+K_2\beta_2+R_{th}K_1\beta_1K_2\beta_2}{K_1\beta_1+K_2\beta_2+R_{th}K_1\beta_1K_2\beta_2}. \tag{8b}$$

Now we consider now a semi-infinite sample whose free surface is located at plane z = 0. If we assume adiabatic boundary conditions at the sample surface (z = 0), the effect of this surface is accounted for by introducing a reflected image of the laser spot with respect to the surface (image method). As in our problem, the laser spot is located at the sample surface, applying the image method means having a laser spot of double power. Accordingly, the temperature in the material is twice the value given by Eqs. (7) for the infinite material

$$T_1(x,y,z)=\frac{P_o}{\pi}\int_0^\infty \delta J_o(\delta r)e^{\beta_1 y}e^{-\beta_2 d}f_1(\delta)d\delta\,, \tag{9a}$$

$$T_2(x,y,z)=\frac{P_o}{2\pi K_2}\int_0^\infty \delta J_o(\delta r)\frac{e^{-\beta_2|y-d|}}{\beta_2}d\delta+\frac{P_o}{2\pi}\int_0^\infty \delta J_o(\delta r)e^{-\beta_2 y}e^{-\beta_2 d}f_2(\delta)d\delta\,. \tag{9b}$$

Finally, if we consider not an ideal point-like heat source but a real Gaussian spot of power P_o and radius a (at $1/e^2$ of the intensity), the temperature in each material is obtained by adding the contribution of each point of the Gaussian spot weighted by its intensity

$$T_1(x,y,z)=\frac{2P_o}{\pi^2 a^2}\int_{-\infty}^{\infty}\int_{-\infty}^{\infty}dx_o dy_o e^{-\frac{2\left[x_o^2+(y_o-d)^2\right]}{a^2}}\int_0^\infty \delta J_o(\delta r_o)e^{\beta_1 y}e^{-\beta_2 y_o}f_1(\delta)d\delta\,, \tag{10a}$$

$$\begin{aligned}T_2(x,y,z)=&\frac{P_o}{2\pi K_2}\int_0^\infty \delta J_o(\delta r_1)\frac{e^{\beta_2 z}}{\beta_2}e^{-\frac{(\delta a)^2}{8}}d\delta+\\&+\frac{P_o}{\pi^2 a^2}\int_{-\infty}^{\infty}\int_{-\infty}^{\infty}dx_o dy_o e^{-\frac{2\left[x_o^2+(y_o-d)^2\right]}{a^2}}\int_0^\infty \delta J_o(\delta r_o)e^{-\beta_2 y}e^{-\beta_2 y_o}f_2(\delta)d\delta\end{aligned}\,, \tag{10b}$$

where $r_o=\sqrt{(x-x_o)^2+z^2}$ and $r_1=\sqrt{x^2+(y-d)^2}$. Eqs (10) give the temperature at any point of each material but its numerical evaluation is rather time consuming since a triple integral is concerned. By considering the surface temperature profile along the y axis, i.e. perpendicular to the interface and crossing the center of the laser spot, the order of the integrals drops, drastically reducing the computing time.

$$T_1(0,y,0)=\frac{P_o}{\pi}\int_0^\infty e^{-\frac{(\delta a)^2}{16}}I_o\left[\frac{(\delta a)^2}{16}\right]e^{\left(\frac{a^2\beta_2^2}{8}-\beta_2 d+\beta_1 y\right)}f_1(\delta)\delta d\delta\,, \tag{11a}$$

$$\begin{aligned}T_2(0,y,0)=&\frac{P_o}{2\pi K_2}\int_0^\infty \delta J_o(\delta|y-d|)\frac{e^{-\frac{(\delta a)^2}{8}}}{\beta_2}d\delta+\\&+\frac{P_o}{2\pi}\int_0^\infty e^{-\frac{(\delta a)^2}{16}}I_o\left[\frac{(\delta a)^2}{16}\right]e^{\left(\frac{a^2\beta_2^2}{8}-\beta_2 d-\beta_2 y\right)}f_2(\delta)\delta d\delta\end{aligned} \tag{11b}$$

Here I_o is the modified Bessel function of order zero.

3. Numerical simulations

In this section, we analyze how the presence two different materials modify the surface temperature if compared to a single medium. Moreover, the lack of perfect thermal contact at the interface between both materials is also studied. In all the simulations, material 2, which is illuminated, is AISI-304 stainless steel (D = 4.0 mm^2/s and K = 15 Wm^{-1}K^{-1}).

Figure 2 shows the calculation of the natural logarithm of the temperature amplitude Ln|T| and the phase Ψ along the y axis for an AISI-304 sample in contact with a material whose thermal conductivity is 5 times smaller than AISI-304 (D = 1.0 mm^2/s and K = 3 Wm^{-1}K^{-1}). The steel sample is illuminated by a Gaussian laser beam with the following parameters: P_o = 0.1 W, a = 0.3 mm, d = 0.6 mm and f = 1 Hz. These parameters have been selected because they are convenient values in IR thermography experiments and moreover, they fulfill the rule of thumb we established to detect and size vertical cracks [14]: $2a \approx d \approx \mu/2$, where $\mu=\sqrt{D/(\pi f)}$ is the thermal diffusion length. Calculations have been performed using Eqs. (11). Four thermal resistances at the interface between the two materials are studied: 0, 10^{-5}, 10^{-4}, 10^{-3} m^{2}K/W. As the room temperature thermal conductivity of air is K_{air} = 0.025 Wm^{-1}K^{-1}, these thermal resistances correspond to air gaps of 0, 0.25, 2.5 and 25 μm. Figure 3 is the same as Fig. 2, but for a medium 1 whose thermal conductivity is 5 times higher than AISI-304 (D =

25 mm^2/s and $K = 75$ $Wm^{-1}K^{-1}$). It is worth noting that we are using the natural logarithm of the temperature since the it discriminates the low temperature values (typically found at the non-illuminated material) better than the temperature itself.

As can be observed in both figures, the interface produces a singularity in both Ln|T| and Ψ when there is a perfect thermal contact ($R_{th} = 0$). However, if there is a lack of adherence between the two media, an abrupt discontinuity appears. We have used the same scale level in Ln|T| and Ψ to clearly show that the jump at the interface is much higher for the former. Accordingly, in the remaining of the paper we will deal only with the temperature amplitude in order to size the thermal resistance. Besides, note that the height of the jump in Ln|T| increases with R_{th}.

Comparing Figs. 2 and 3, the main difference is that for a fixed value of the thermal resistance the jump in Ln|T| is higher for the good thermal conductor than for the poor thermal conductor. For instance, the thermal resistance of 10^{-5} m^2K/W, the red lines in both figures, is barely distinguishable from a perfect thermal contact when material 1 is a worse thermal conductor than AISI-304, but produces a clear jump of 0.96 if material 1 is a better thermal conductor than AISI-304. This result can be explained after analyzing Eqs. (8). Actually, the thermal resistance is correlated to K_1 and K_2 through the factor $R_{th}K_1K_2$. This means that for a fixed value of material 2, the higher the value of K_1, the lower the R_{th} value that can be detected.

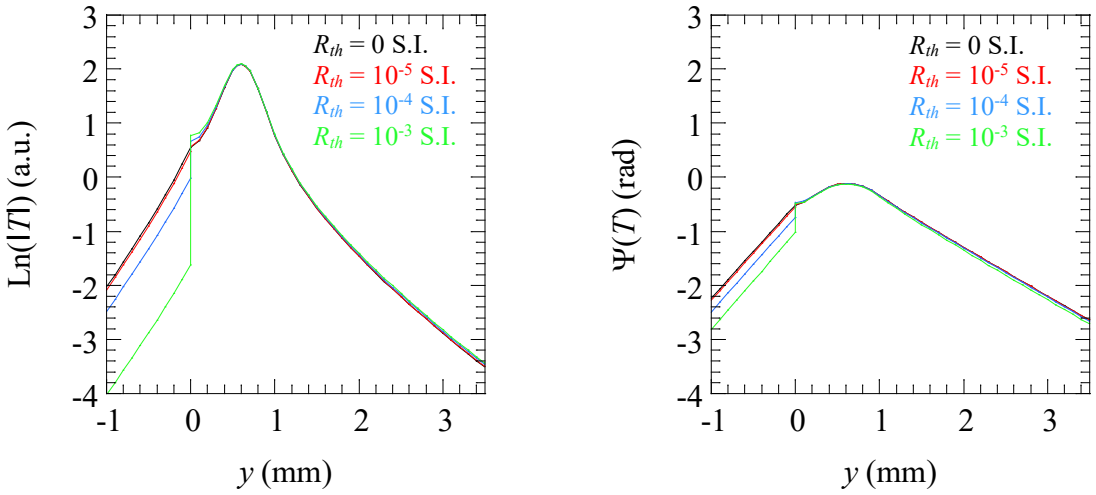

Figure 2. Simulation of the natural logarithm of the temperature amplitude, Ln(|T|), and phase, Ψ(T), along the y axis for an AISI-304 sample ($D_2 = 4$ mm^2/s and $K_2 = 15$ $Wm^{-1}K^{-1}$) sample in contact with a worse thermal conductor ($D_1 = 1$ mm^2/s and $K_1 = 3$ $Wm^{-1}K^{-1}$). The AISI-304 sample is illuminated by a modulated laser beam: $P_o = 0.1$ W, $a = 0.3$ mm, $d = 0.6$ mm and $f = 1$ Hz. The effect of the thermal resistance R_{th} (m^2K/W) at the interface ($y = 0$) is shown.

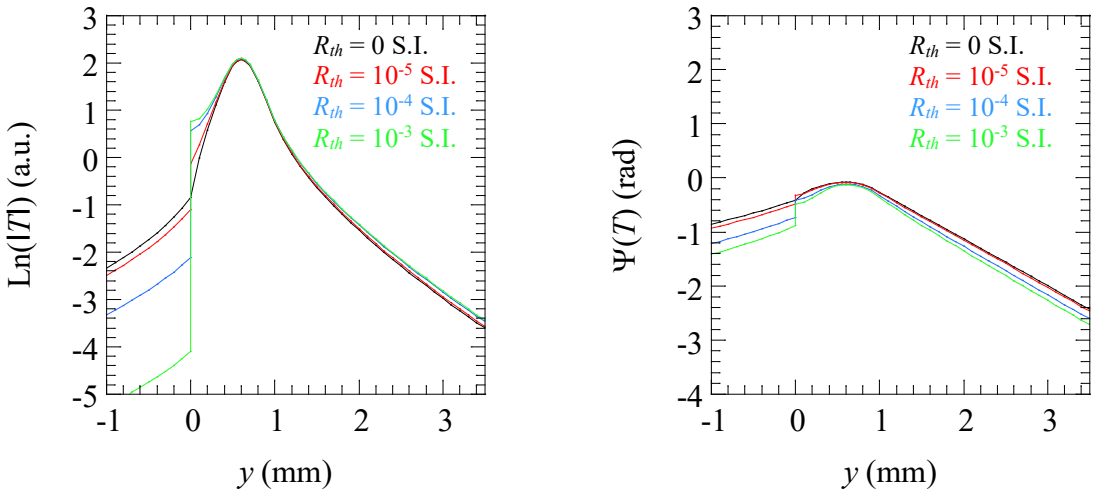

Figure 3. The same as in Fig. 2, when medium 1 is a better thermal conductor (D_1 = 25 mm^2/s and K_1 = 75 Wm^{-1}K^{-1}) than medium 2.

In order to quantify the height of the temperature jump at the crack position we introduce the temperature contrast in Ln|T|, Δ , which we define as

$$\Delta = Ln\left(\left|T_2(0,0,0)\right|\right) - Ln\left(\left|T_1(0,0,0)\right|\right). \qquad (18)$$

Note that this contrast is independent of the laser power P_o.

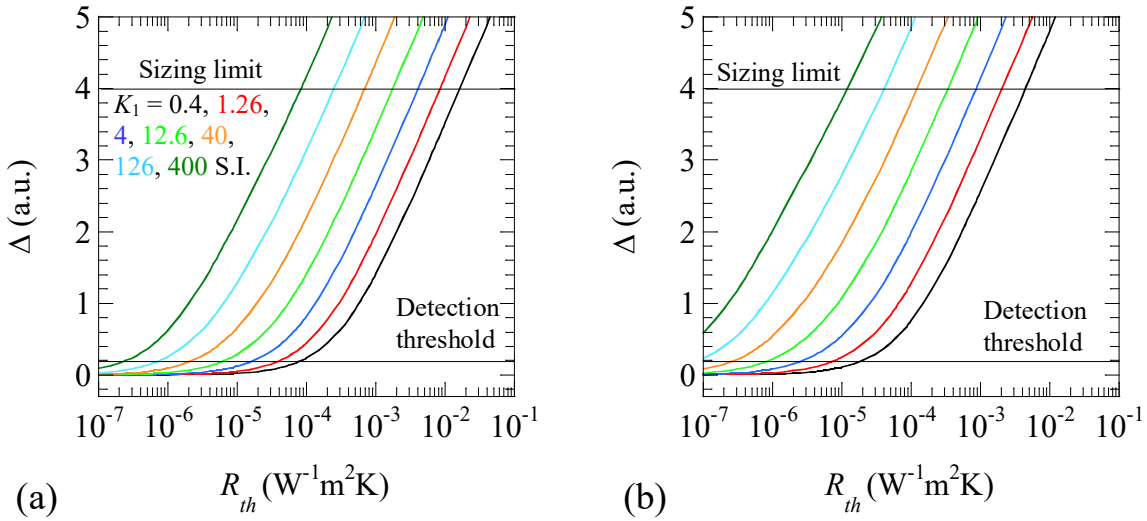

Figure 4. Simulation of the dependence of the temperature contrast Δ on the thermal contact resistance R_{th}. Calculations are performed by keeping fixed material 2 (AISI-304) and varying the thermal properties of material 1. The lower horizontal line indicates the threshold to detect the discontinuity at the interface and the upper one the limit to size the discontinuity. The experimental parameters are: (a) a = 0.3 mm, d = 0.6 mm and f = 1 Hz and (b) a = 0.03 mm, d = 0.06 mm and f = 100 Hz.

In Fig. 4 we show the simulations of the temperature contrast Δ as a function of the thermal contact resistance R_{th}. In the simulations, material 2 is AISI-304 while the thermal conductivity of material 1 varies from 0.4 (thermal insulators like polymers) to 400 Wm^{-1}K^{-1} (good thermal conductors like copper) in multiplying steps of $\sqrt{10}$. The corresponding thermal

diffusivity also varies in steps of $\sqrt{10}$ from 0.1 to 100 mm^2/s. In Fig. 4a the experimental parameters we have used in the numerical calculations are a = 0.3 mm, d = 0.6 mm and f = 1 Hz. The first thing to be mentioned is the general rule that low R_{th} are better detected (produce higher Δ) when material 1 is a good thermal conductor than when it is an insulator. For instance, a thermal resistance of 10^{-5} m^{2}K/W (equivalent to an air gap of L = 0.25 μm) remains undetected when material 1 is an insulator with K_1 = 0.4 Wm^{-1}K^{-1} (see the black line in Fig. 4a), but produces a thermal contrast as high as Δ = 2.17 for K_1 = 400 Wm^{-1}K^{-1} (see the dark green line in Fig. 4a). On the other hand, note that for a given material 1 (a given color in Fig. 4a), there is a minimum R_{th} value below which the temperature contrast becomes negligible and therefore the discontinuity at the interface remains undetected. Taking into account the experimental noise, we have stablished a quite conservative detection threshold when the temperature contrast is Δ = 0.2 (see Fig. 4a). Finally, as R_{th} increases the temperature contrast rises monotonously, indicating that these air gaps are easily detectable. However, as high Δ means that the temperature in material 1 is very low, these wide air gaps cannot be sized precisely due to the experimental noise. Accordingly, we have stablished a sizing threshold $\Delta \approx 4$, which corresponds to a temperature in material 1 around 15 mK. Accordingly, for higher thermal contrasts the air gap is clearly identified but cannot be sized accurately.

Figure 4b is the same as Fig. 4a, but we increasing the frequency two orders of magnitude: f = 100 Hz. Moreover, in order to fulfill the relationship $2a \approx d \approx \mu/2$, which provides the best experimental conditions to size vertical cracks, we have reduced consequently a and d one order of magnitude: a = 30 μm, d = 60 μm. As can be seen, as the modulation frequency is increased by two orders of magnitude, the thermal contrast Δ is displaced to lower R_{th} values by almost one order of magnitude. This result means that high frequencies are better suited to detect and size extremely narrow discontinuities. Anyway, note that although focusing a cw laser to a radius of 30 μm and positioning its center at 60 μm from the interface between two media is easy, the spatial resolution of the current IR video cameras is not enough to work so close to the interface. For instance, our IR camera with a microscope lens has a resolution of 30 μm, which is not enough to deal with frequencies higher than 10 Hz.

The method we propose to size the thermal resistance at the interface between two different materials consists in fitting the temperature profile across the interface to the analytical model given by Eqs. (11).

4. Experimental results

Figure 5 shows the scheme of the experimental setup. A cw laser (532 nm), whose intensity is modulated by an acousto-optic modulator, is directed to the sample surface by means of a mirror and a germanium window, which is opaque to visible light but transparent to IR wavelengths. We focus the laser beam onto the sample surface using a 10 cm focal length lens. We adjust the laser power to obtain a similar temperature rise at the center of the laser spot of about 5-10 K. An IR video camera (FLIR, model SC7500) with an InSb detector operating in the 3 - 5 μm spectral range and equipped with a lock-in module delivers the amplitude and phase of the surface temperature. A microscope lens improves the spatial resolution so that each pixel measures the average temperature over a square of 30 μm in side. To enhance the signal to noise ratio we record a large number of images, since in lock-in measurements the average noise level in temperature amplitude is inversely proportional to the square root of the number of images collected for the lock-in analysis [22]. In our case, as we record 2×10^4 images at a frame rate of 350 images/s (about 1 minute) the noise level of the data is kept below 1 mK.

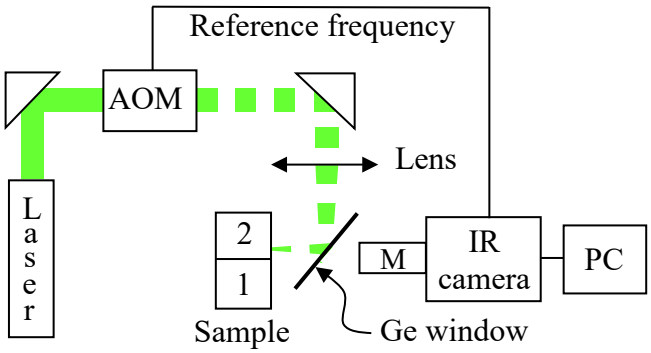

Figure 5. Diagram of the experimental setup. AOM is the acousto-optic modulator and M is the microscope lens. The laser hits material 2.

To verify the method we have proposed to size the thermal resistance at the interface between two materials with different thermal properties, we have put in contact under pressure a parallelepiped block of AISI-304 stainless steel with another parallelepiped piece of a different material. First, we use a thermal insulator, polyether-ether-ketone (PEEK, $D = 0.18$ mm^2/s and $K = 0.25$ Wm^{-1}K^{-1}) and then, a good thermal conductor, copper ($D = 116$ mm^2/s and $K = 400$ Wm^{-1}K^{-1}). The surfaces in contact have mirror like finishing. In order to calibrate the air gap between the blocks, we insert calibrated nickel tapes of micronic thickness between them (see Fig. 6). In the two configurations (AISI-304 + PEEK and AISI-304 + Cu) we illuminate the steel piece, as we did in the simulations. We deposit a thin graphite layer a few microns thick onto the surface of the two materials in order to increase the absorption to the heating laser and to make the emissivity to infrared equal in both materials.

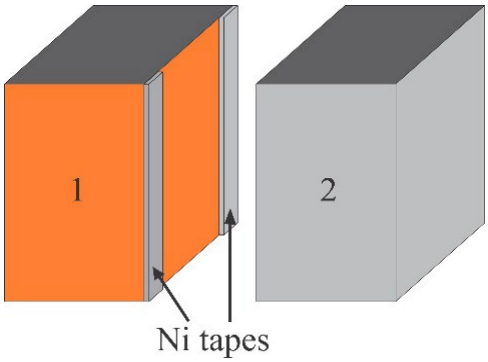

Figure 6. Diagram of the infinite interface between two materials manufactured for the experiment: Two thin Ni tapes of the same thickness are sandwiched between two blocks of different materials. The upper surface of both blocks is covered by a thin graphite layer.

We start analyzing the results corresponding to the combination of AISI-304 and PEEK. All measurements have been performed with the same experimental parameters: $f = 0.42$ Hz, $d \approx 0.35$ mm and $a \approx 0.20$ mm. Using nickel tapes of several thicknesses we have obtained the following calibrated interface air gap widths: $L = 0$, 2.5, 5, 10, 20, 30 and 50 μm. The amplitude thermogram shown in Fig. 7a corresponds to the direct contact between the two blocks ($L = 0$ μm). As can be observed, there is a horizontal line at the boundary between the two materials. Unlike in the case of infinite vertical cracks in the same material, where a clear line in the

thermogram indicates a thermal discontinuity and therefore a thermal resistance [13,14], in the case of the junction between two different materials there is always a line indicating the transition from a material to the other one, due to the difference in their thermal properties. Accordingly, just looking at the IR thermogram it is impossible to assess whether there is a perfect thermal contact or there is a thermal resistance between them. To size the thermal resistances we analyzed the profiles of Ln(|T|) along the y axis for all air gaps, which are plotted in Fig. 7b. Dots are the experimental data that for each profile have been shifted to better appreciate the jump at the crack. They exhibit a very low noise level due to lock-in averaging. Actually, at the longest distances shown in Fig. 7b, y = -1 and +4 mm, the temperature is around 20 mK, but, as said before, the noise level remains lower than 1 mK. The continuous lines are the least squares fits to Eqs. (11) using four free parameters: P_o, a, d and R_{th}. The retrieved thermal resistance values are R_{th} = (2.3±2.9)×10^{-5}, (1.10±0.17)×10^{-4}, (1.64±0.15)×10^{-4}, (3.3±0.2)×10^{-4}, (8.4±0.3)×10^{-4}, (1.14±0.05)×10^{-3} and (1.61±0.06)×10^{-3} m^{2}K/W, which correspond to the following air widths, L = 0.57±0.71, 2.8±0.4, 4.1±0.4, 8.5±0.4, 21±1, 29±1 and 41±2 μm respectively. They are in good agreement with the nominal values of the nickel tapes thicknesses, except for the case of direct contact between both blocks. Note that the uncertainty is around 5% for interface widths verifying $L \geq 10$ μm. However, as the width reduces the uncertainty increases (9%, 15% and 124% for L = 5, 2.5 and 0 μm, respectively). This is due to the reduction in the temperature contrast at the interface. In the case of direct contact (L = 0 μm), the fitting procedure is able to give a value of the thermal resistance, but the uncertainty is so high that the method cannot distinguish widths in the range 0-1 μm. This result is in agreement with the simulations given in Fig. 4a, where for temperature contrasts below 0.2 the thermal resistance cannot be detected. On the other hand, in all fittings the retrieved values of a and d are in the range d = 0.33-0.37 mm and a = 0.18-0.22 mm, which are very close to the values measured optically.

Then, we studied the IR measurements corresponding to the ensemble of AISI-304 with copper. We use the same experimental parameters for all the measurements performed on this combination: f = 0.19 Hz, $d \approx$ 0.30 mm and $a \approx$ 0.15 mm. In Fig. 8a, we show the amplitude thermogram corresponding to the direct contact between steel and copper. As before, there is a clear border indicating the change of the thermal properties between both materials, but looking at this figure, it is not possible to evaluate whether the thermal contact is perfect. Figure 8b shows the temperature profiles along the y axis for seven air gap widths: 0, 1, 2.5, 5 and 10 μm. Dots are the experimental data and the continuous lines are the least squares fits to Eqs. (11). Note that even for a tightly contact between the two blocks (L = 0 μm) a net jump appears at the interface. This result confirms the prediction of section 3 that extremely narrow cracks are easily detected if the two materials are very good thermal conductors. The retrieved value of its thermal resistance is R_{th} = (4.3±0.4)×10^{-5} m^{2}K/W, which corresponds to an air gap of L = 1.1±0.1 μm. By fitting other perpendicular profiles on the same sample we obtain always interface widths in the range L = 0.7-1.2 μm. This is the closest interface that we can manufacture in cm-scale metallic samples. Simulations indicate that obtaining an almost perfect thermal contact in steel-copper ensembles using the same experimental parameters requires the interface width to be $L \leq$ 10 nm (see de dark green line in Fig. 4a), which are not possible to machine. The fittings corresponding to the remaining samples give the following thermal resistances, R_{th} = (7.4±0.6)×10^{-5}, (9.1±0.7)×10^{-5}, (1.61±0.14)×10^{-4} and (2.4±0.3)×10^{-4} m^{2}K/W, which correspond to the following air gap widths, L = 1.86±0.16, 2.27±0.18, 4.0±0.4 and 6.1±0.6 μm respectively. In all fittings the retrieved values of a and d are in the range d = 0.27-0.33 mm and a = 0.13-0.17 mm, very close to the values measured optically.

Although the retrieved values of the air gap width are good, they are worse than those obtained in the couple steel/PEEK. The reason for that is associated to the temperature data in the copper region as given in Fig. 8b. On the one hand, far away from the interface (-2 mm < y

< -1 mm) the temperature level is around 10 mK for $L = 0$ and falls down to 3 mK for $L = 10$ μm. Therefore they are noisier than in the case of PEEK. This is due to the huge jump at the interface position when material 1 is a good thermal conductor. On the other hand, near the interface (-0.5 mm < y < 0 mm) the temperature does not exhibit the expected sharp discontinuity at the interface but a smooth transition involving around 15 pixels. This result is due to the imperfect imaging system of the IR camera (diffraction, multiple reflections, optical aberrations…). The so-called Point Spread Function (PSF) describes the response of an imaging system to a point source or point object, and depends on the lens quality [23]. This effect is more noticeable as the temperature difference at the interface increases. Actually, this effect is also present in the PEEK temperature data (see Fig. 6b), but only involves 2 or 3 pixels. Accordingly, the effect of the PSF is negligible in the fittings in the steel/PEEK couple, but becomes significant in the steel/Cu ensemble. In this way, the retrieved values of the thermal resistance are less accurate as the jump at the interface increases. Both, the low temperature level together with the PSF are the reason why we established a sizing limit in Fig. 3, indicating it is impossible to get accurate R_{th} values when the temperature contrast verifies $\Delta > 4$. This is just what happens for $L \geq 5$ μm in the couple steel/Cu for which the temperature contrast verifies $\Delta \approx 4.5$-5, as can be seen in Fig. 8b. This means that this method is not able to size air gaps thicker than 5 μm in steel/Cu ensembles. Accordingly, the retrieved value for $L = 5$ μm is still acceptable ($L = 4.0$ μm), but becomes just an estimation for $L = 10$ μm ($L = 6.0$ μm).

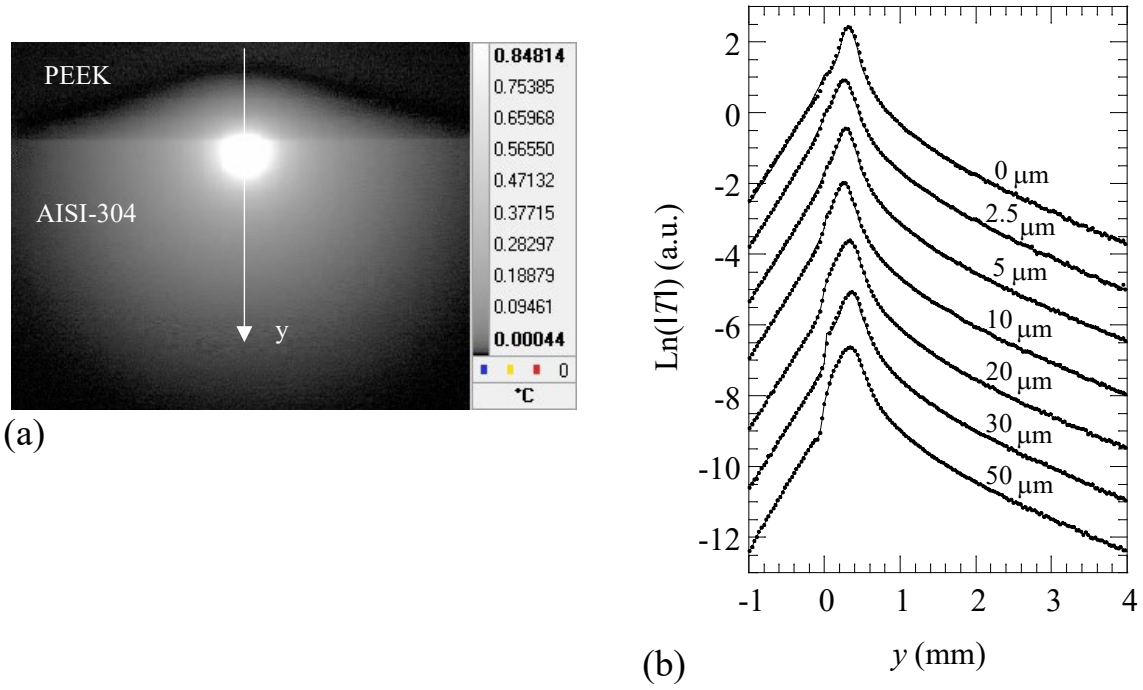

Figure 7. (a) Amplitude thermogram at 0.42 Hz for an AISI-304 block in direct contact with a PEEK block ($L = 0$ μm). (b) Natural logarithm of the surface temperature amplitude along the y axis for seven interface widths. The interface is placed at $y = 0$. Dots correspond to experimental data and continuous lines to the fit to Eqs. (11). The values of Ln|T| for each profile have been shifted to better appreciate the jumps at the interface.

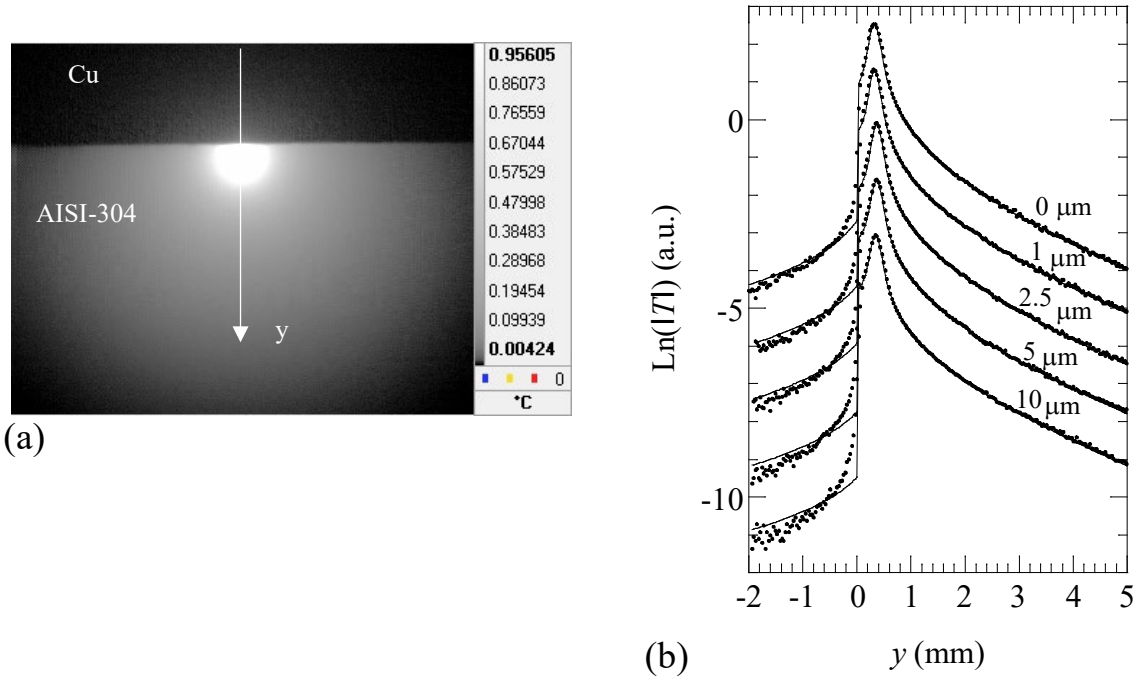

Figure 8. (a) Amplitude thermogram at 0.42 Hz for an AISI-304 block in direct contact with a copper block (L = 0 μm). (b) Natural logarithm of the surface temperature amplitude along the y axis for five interface widths. The interface is placed at y = 0. Dots correspond to experimental data and continuous lines to the fit to Eqs. (11). The values of Ln|T| for each profile have been shifted to distinguish the jump at the interface.

5. Conclusions

In this work, we addressed the issue of sizing the vertical interface between two different media using lock-in thermography with laser spot heating. First, we found an analytical expression for the surface temperature of the two-media when a modulated and focused laser beam impinges near the interface. This interface between the two media produces a singularity in the temperature field, just at the interface position, due to the difference in their thermal properties. Besides, if the thermal contact between the two materials is not perfect, an abrupt discontinuity in the temperature at the interface is added. The method we propose to size the thermal resistance consists in fitting the temperature profile across the interface to the analytical model. The validity of the model has been tested experimentally by performing lock-in thermography measurements on steel/PEEK and steel/copper ensembles with calibrated interface widths. By fitting the temperature amplitude profiles across the interface to the model, the air gap width at the interface is obtained. The good agreement between the optically calibrated width and the retrieved one confirms the validity of the method. The results indicate that it is easier to detect narrow interfaces in good thermal conductors than in insulators. Due to the diffraction limit and the spatial resolution of nowadays cameras, IR thermography is restricted to size interfaces widths down to tenths of micron ($R_{th} \approx 10^{-5}$ m^{2}K/W). Characterizing interface widths in the nanometer scale ($R_{th} \approx 10^{-8}$-10^{-9} m^{2}K/W), as is the case of grain boundaries in polycristaline samples or composite materials, requires a high modulation frequencies (MHz) and a point-like laser spot. Modulated photothermal reflectance (MPR) is

an ideal technique to reach the nanometer limit. It is worth mentioning that the method proposed in this manuscript is directly applicable to MPR.

Acknowledgments

This work has been supported by Ministerio de Economía y Competitividad (DPI2016-77719-R, AEI/FEDER, UE), by Universidad del País Vasco UPV/EHU (GIU16/33) and by Conacyt (Beca Mixta 2017 Movilidad en el extranjero).

References

[1] Kubiak EJ. Infrared detection of fatigue cracks and other near-surface defects. Appl. Opt. 1968;7(9):1743-8.
[2] Mendioroz A, Celorrio R and Salazar A. Ultrasound excited thermography: An efficient tool for the characterization of vertical cracks. Meas. Sci. Technol. 2017;28:112001.
[3] Oswald-Tranta B. Thermoinductive investigations of magnetic materials for surface cracks. QIRT Journal 2004;1:33-46.
[4] Jäckel P and Netzelmann U. The influence of external magnetic fields on crack contrast in magnetic steel detected by induction thermography. QIRT Journal 2013;10:237-247.
[5] Grice KR, Inglehart LJ, Favro LD, Kuo PK and Thomas RL. Thermal wave imaging of closed cracks in opaque solids. J. Appl. Phys. 1983;54:6245-55.
[6] Mansanares AM, Velinov T, Bozoki Z, Fournier D and Boccara AC. Photothermal microscopy: Thermal contrast at grain interface in sintered metallic materials. J. Appl. Phys. 1994;75:3344-50.
[7] Li T, Almond P, Andrew D and Rees S. Crack imaging by scanning pulsed laser spot thermography. NDT&E Int 2011;44:216-225.
[8] Schlichting J, Maierhofer C, Kreutzbruck M. Crack sizing by laser excited thermography. NDT&E Int 2012;45(1):133–40.
[9] Streza M, Fedala Y, Roger JP, Tessier G and Boue C. Heat transfer modelling for surface crack depth evaluation. Meas. Sci. Technol. 2013;24:045602.
[10] Boué C and Holé S. Open crack depth sizing by multi-speed continuous laser stimulated lock-in thermography. Meas. Sci. Technol. 2017;28:065901.
[11] Lepoutre F, Balageas D, Forge Ph, Hirschi S, Joulaud JL, Rochais D and Chen FC. Micron-scale thermal characterizations of interfaces parallel or perpendicular to the surface. J. Appl. Phys. 1995;78:2208-23.
[12] Ocariz A, Sanchez-Lavega A, Salazar A, Fournier D and Boccara AC. Photothermal characterization of vertical and slanted thermal barriers: A quantitative comparison of mirage, thermoreflectance and infrared radiometry. J. Appl. Phys. 1996;80:2968-82.
[13] Pech-May NW, Oleaga A, Mendioroz A, Omella AJ, Celorrio R and Salazar A. Vertical cracks characterization using lock-in thermography: I infinite cracks. Meas. Sci. Technol. 2014;25:115601.
[14] Pech-May NW, Oleaga A, Mendioroz A and Salazar A. Fast characterization of the width of vertical cracks using pulsed laser spot infrared thermography. J Nondestruct. Eval. 2016;35:22.
[15] Hua Z and Ban H, A new measurement approach for interface thermal resistance using frequency-scan photothermal reflectance technique. Int. J. Therm. Sci. 2017;11:59-67.
[16] Sanchez-Lavega A, Forge Ph, Salazar A and Ocariz A. Photothermal mirage characterization of vertical interfaces separating two different media. J. Appl. Phys. 1996;79:599-608.
[17] Bracewell R N 1986 *The Fourier Transform and its Applications* (McGraw-Hill) p. 244.
[18] Rosencwaig A, Opsal J, Smith WL and Willenborg DL. Detection of thermal waves through optical reflectance. Appl. Phy. Lett. 1985;46:1013-1015.
[19] Hartmann J, Costello M and Reichling M. Influence of thermal barriers on heat flow in high quality chemical vapour deposited diamond. Phys. Rev. Lett. 1998;80:117-120.
[20] McDonald FA, Wetsel GC and Jamieson GE. Photothermal beam-deflection imaging of vertical interfaces in solids. Can. J. Phys. 1986;64:1265-8.
[21] Carslaw H S and Jaeger J C 1959 *Conduction of Heat in Solids* (Oxford: Oxford University Press) p. 20.
[22] Breitenstein O and Langenkamp M 2003 *Lock-in Thermography* (Berlin: Springer) p. 32.

[23] Shaw PJ and Rawlins DJ. (August 1991). The point-spread function of a confocal microscope: its measurement and use in deconvolution of 3-D data. J. of Microsc. 1991;163:151-165.

Figure captions

Figure 1. Geometry of the problem showing the vertical interface (in grey) between medium 1 and 2 and illuminated by a Gaussian laser beam.

Figure 2. Simulation of the natural logarithm of the temperature amplitude, Ln(|T|), and phase, $\Psi(T)$, along the y axis for an AISI-304 sample (D_2 = 4 mm^2/s and K_2 = 15 Wm^{-1}K^{-1}) sample in contact with a worse thermal conductor (D_1 = 1 mm^2/s and K_1 = 3 Wm^{-1}K^{-1}). The AISI-304 sample is illuminated by a modulated laser beam: P_o = 0.1 W, a = 0.3 mm, d = 0.6 mm and f = 1 Hz. The effect of the thermal resistance R_{th} (m^{2}K/W) at the interface (y = 0) is shown.

Figure 3. The same as in Fig. 2, when medium 1 is a better thermal conductor (D = 25 mm^2/s and K = 75 Wm^{-1}K^{-1}) than medium 2.

Figure 4. Simulation of the dependence of the temperature contrast Δ on the thermal contact resistance R_{th}. Calculations are performed by keeping fixed material 2 (AISI-304) and varying the thermal properties of material 1. The lower horizontal line indicates the threshold to detect the discontinuity at the interface and the upper one the limit to size the discontinuity. The experimental parameters are: (a) a = 0.3 mm, d = 0.6 mm and f = 1 Hz and (b) a = 0.03 mm, d = 0.06 mm and f = 100 Hz.

Figure 5. Diagram of the experimental setup. AOM is the acousto-optic modulator and M is the microscope lens. The laser hits material 2.

Figure 6. Diagram of the infinite interface between two materials manufactured for the experiment: Two thin Ni tapes of the same thickness are sandwiched between two blocks of different materials. The upper surface of both blocks is covered by a thin graphite layer.

Figure 7. (a) Amplitude thermogram at 0.42 Hz for an AISI-304 block in direct contact with a PEEK block (L = 0 μm). (b) Natural logarithm of the surface temperature amplitude along the y axis for several interface widths. The interface is placed at y = 0. Dots correspond to experimental data and continuous lines to the fit to Eqs. (11). The values of Ln|T| for each profile have been shifted to better appreciate the jumps at the interface.

Figure 8. (a) Amplitude thermogram at 0.42 Hz for an AISI-304 block in direct contact with a copper block (L = 0 μm). (b) Natural logarithm of the surface temperature amplitude along the y axis for five interface widths. The interface is placed at y = 0. Dots correspond to experimental data and continuous lines to the fit to Eqs. (11). The values of Ln|T| for each profile have been shifted to distinguish the jump at the interface.